Load-sharing and kinematics of the human cervical spine under multi-axial transverse shear loading: combined experimental and computational investigation

T. Whyte
Orthopaedic and Injury Biomechanics Group, Departments of Mechanical Engineering and Orthopaedics, The School of Biomedical Engineering and International Collaboration on Repair Discoveries, University of British Columbia, Vancouver, Canada
Neuroscience Research Australia, Sydney, Australia
Margarete Ainsworth Building, Barker St, Randwick, NSW, 2031, Australia
t.whyte@neura.edu.au

J.B. Barker
Department of Mechanical and Mechatronics Engineering, University of Waterloo, Waterloo, Canada
200 University Ave W, Waterloo, ON, N2L 3G1, Canada
jeffrey.barker@uwaterloo.ca

D.S. Cronin
Department of Mechanical and Mechatronics Engineering, University of Waterloo, Waterloo, Canada
200 University Ave W, Waterloo, ON, N2L 3G1, Canada
duane.cronin@uwaterloo.ca

G.A. Dumas
Department of Mechanical and Materials Engineering, Queen's University, Kingston, Canada
130 Stuart Street Queen's University Kingston, ON, K7L 3N6, Canada
genevieve.dumas@queensu.ca

L.-P. Nolte
ARTORG Center for Biomedical Engineering Research, University of Bern, Bern, Switzerland
Freiburgstrasse 3, 3010 Bern, Switzerland
lutz.nolte@artorg.unibe.ch

P.A. Cripton
Orthopaedic and Injury Biomechanics Group, Departments of Mechanical Engineering and Orthopaedics, The School of Biomedical Engineering and International Collaboration on Repair Discoveries, University of British Columbia, Vancouver, Canada
6250 Applied Science Lane, Vancouver, BC, V6T 1Z4, Canada
peter.cripton@ubc.ca

Keywords: cervical spine; biomechanics; ex vivo; shear; compression; load-sharing; kinematics

Word Count: 6057 (introduction to conclusion)

ABSTRACT

The cervical spine experiences shear forces during everyday activities and injurious events yet there is a paucity of biomechanical data characterizing the cervical spine under shear loading. This study aimed to 1) characterise load transmission paths and kinematics of the subaxial cervical spine under shear loading, and 2) assess a contemporary finite element cervical spine model using this data.

Subaxial functional spinal units (FSUs) were subjected to anterior, posterior and lateral shear forces (200 N) applied with and without superimposed axial compression preload (200 N) while monitoring spine kinematics. Load transmission paths were identified using strain gauges on the anterior vertebral body and lateral masses and a disc pressure sensor.

Experimental conditions were simulated with cervical spine finite element model FSUs (GHBMC M50 version 5.0). The mean kinematics, vertebral body strains and disc pressures were compared to experimental results.

The shear force-displacement response typically demonstrated a toe region followed by a linear response, with higher stiffness in the anterior shear direction relative to lateral and posterior shear. Compressive axial preload decreased posterior and lateral shear stiffness and increased anterior shear stiffness. Load transmission patterns and kinematics suggest the facet joints play a key role in limiting anterior shear while the disc governs motion in posterior shear. The main cervical spine shear responses and trends are faithfully predicted by the GHBMC finite element cervical spine model.

These basic cervical spine biomechanics and the computational model can provide insight into mechanisms for facet dislocation in high severity impacts, and tissue distraction in low severity impacts.

INTRODUCTION

The cervical spine can be subjected to considerable shear forces from physiologic and impact loading, owing to the relative slenderness of the neck, the weight of the head and the deceleration of the following torso in a head-first impact. In a direct impact to the head (from a fall or dive), shear forces can develop and may play a significant role in the occurrence of facet dislocation injuries [1,2], a traumatic injury often associated with catastrophic damage to the spinal cord. Shear forces are also present in the cervical spine from inertial loading of the head due to acceleration of the torso, as occurs in cases of whiplash associated disorder (WAD) [3,4], typically in combination with a bending moment and axial compression. Surrounding neck musculature likely supports some of the applied loads but the shear component may still be large (100-2000 N) [5–7]. Despite these important circumstances where shear loading plays a role in cervical spine injury mechanisms, there is a paucity of knowledge regarding the basic biomechanics and load-sharing of the cervical spine in shear. Panjabi *et al.* [8], Moroney *et al.* [9], Shea *et al.* [10], Siegmund *et al.* [11] and Dowling-Medley *et al.* [12] have characterised the kinematic response of cervical functional spinal units (FSUs), consisting of two or three adjacent vertebrae and the disc and ligament tissues that connect them, subjected to varying combinations of anteriorly, posteriorly and laterally directed shear forces and to various simulated injuries. Although this previous work provides insight into the shear response of the cervical spine, there are limitations associated with these studies and some basic issues that have not been investigated.

Force must be applied to a motion segment in the mid-disc plane to result in pure shear forces [13]. Other application points are known to subject the FSU to combined shear force and moment loading [9,14,15]. Only Moroney *et al.* [9] and Dowling-Medley *et al.* [12] have applied

pure shear forces in this way, meaning the cervical spine response to shear force alone is difficult to isolate in other studies. Further, both Moroney *et al.* [9] and Panjabi *et al.* [8] applied relatively low magnitude shear forces (20 and 50 N, respectively). These are much smaller than those expected *in vivo* for some physiologic (up to 135 N [6]) or traumatic (1100-2000 N [5]) loading scenarios. Additionally, although small preloads have been included in some previous investigations [8,9], the influence of axial preload representative of that present *in vivo* (100-1000 N [6]) has not been systematically investigated for pure shear loading. Under combined loads with shear, the effect of preload differs between studies [11,16]. Furthermore, there is no experimental data to our knowledge about load-sharing and intervertebral disc biomechanics as a function of applied shear forces in the cervical spine.

Experimental biomechanical data sets detailing the cervical spine's basic biomechanical response to pure shear loads could be used to validate and improve contemporary computational human body models. These models provide the ability to predict injury and design strategies and products for injury prevention in complex load scenarios [17]. The lack of pure shear experiments currently available has provided an obstacle to complete validation of cervical spine computational models for the basic biomechanics of the neck.

Several detailed finite element models of the cervical spine have been developed, and are often assessed at the motion segment level for extension, flexion, lateral bending, and axial rotation modes of loading [18–23]. Only one of those models was assessed in any form of shear loading [23], with the applied load being a combination of shear and flexion or extension [10]. Contemporary FE models of the neck include the Total Human Model for Safety (THUMS), Collaborative Human Advanced Research Models (CHARM) and the Global Human Body Models Consortium (GHBMC) human body models [17], none of which have been assessed for

shear loading at the motion segment levels. Although the GHBMC model has been assessed with over 20 different tests at the motion segment level [22] and the full neck [24], the paucity of shear data and conflicting results among what is available has not enabled general model assessment or validation. The shear response may be important in high-severity traumatic loading leading to catastrophic tissue failure, facet dislocation and spinal cord injury, and lower severity impact loading such as is associated with WAD, where sub-catastrophic distractions of tissues may lead to chronic pain [25].

The objectives of this study was to (1) experimentally characterise cervical spine kinematics and load-sharing mechanisms as a function of anterior, posterior and lateral shear force application with and without axial preload and (2) objectively compare the cervical spine shear response to the response of a contemporary finite element model of the cervical spine.

EXPERIMENTAL MATERIALS AND METHODS

Specimens

Seven two-vertebra cervical functional spinal units (FSUs), see Table 1, were harvested, fresh-frozen and prepared by removing all muscle tissue while leaving all ligamentous and bony structure intact. The dens was removed from the C2 specimens to simplify potting for experimental testing. Screws were inserted partly into the most cranial and caudal parts of the vertebrae of the FSUs to improve anchoring of the specimen in polymethylmethacrylate (PMMA) potting, taking care not to contact the intervertebral disc (IVD), facet joints or capsule with the screws or PMMA. The natural lordotic posture of the specimen was maintained. Water was frequently applied to the exposed specimen surfaces to prevent the anatomic structures from dehydrating.

Not all donor information was provided. None of the donors had suffered trauma involving the

head or cervical spine nor had they suffered diseases associated with changes in bone quality. The specimens were screened for severe degeneration or other bony abnormality by X-ray.

Table 1 Specimen details and experimental data collected for each specimen (VB is vertebral body, LM is lateral mass, Pre is axial preload, A is anterior shear, P is posterior shear, L is left shear, R is right shear)

Specimen ID	**Spinal level**	**Age**	**Sex**	**Cause of death**	**Experimental data collected**							
					Kinematics		VB strain		LM Strain		Disc Pressure	
					No Pre	Pre	No Pre	Pre	No Pre	Pre	No Pre	Pre
1778	C2-3	83	Male	Cancer	A, P, L, R	A, P, L, R	A, P, L, R	A, P, L, R	A, P, L, R	A, P, L, R	A, P, L, R	A, P, L, R
1778	C4-5	83	Male	Cancer	A, P, L, R	A, P, L, R	A, P, L, R	A, P, L, R	A, P, L, R	A, P, L, R	A, P, R	A, P, R
1799	C2-3	80	Female	Ovarian cancer	A, P, L, R	A, P, L, R	A, P, L, R	A, P, L, R	A, P, L, R	A, P, L, R	A, P, L, R	A, P, L, R
1799	C4-5	80	Female	Ovarian cancer	A, P, R	A, P, R	A, P, R	A, P, R	A, P, R	A, R	A, P, R	A, P, R
1800	C6-7	82	Female	Lung embolism	A, P, L, R	A, P, L, R	A, P, L, R	A, P, L, R	A, P, L, R	A, P, L, R	A, P, L, R	A, P, L, R
1803	C3-4	Unknown	Unknown	Unknown	A, P, L, R	A, P, L, R	A, P, L, R	A, P, L, R	A, P, R	A, P, L, R	A, P, R	P, L
1803	C5-6	Unknown	Unknown	Unknown	A, P, L, R	A, P, L, R	A, P, L, R	A, P, L, R	A, P, L, R	A, P, L, R	A, P, L, R	P, L, R

Load transmission instrumentation

Vertebral strain and disc pressure were measured to determine loading routes through the FSU. Triaxial strain gauge rosettes (FRA-1-11, Tokyo Kenkyujo Co. Ltd., Tokyo, Japan) arranged in a rectangular configuration (0°, 45° and 90°) were applied to the anterior surface of the caudal vertebral body and on the lateral masses beneath the left and right facet joints. Each gauge had a nominal resistance of 120 Ω, gauge length 1 mm, gauge factor of approximately 2.1 and maximum extensibility of 3%. The area for application was prepared using a scalpel to remove

ligamentous tissue periosteum and an absorbent swab to remove fluid. Cyanoacrylate adhesive (Histoacryl Braun, Melsungen, Germany) was used to bond the rosettes to the bone.

A disc-shaped miniature pressure sensor of diameter 1.5 mm and thickness 0.3 mm was used to measure intradiscal pressure. The sensor was inserted into the centre of the intervertebral disc using a 2.2 mm diameter needle. The needle was then removed, leaving only the sensor lead wire passing through the disc annulus [26]. Strain and pressure signals were sampled at 10 Hz. Principal strain magnitudes and their orientation were calculated for each rosette.

Load application and test protocol

Anterior, posterior, left and right shear forces were applied to each specimen using an adjustable loading rig (Fig. 1) and a uniaxial servohydraulic materials testing machine (Model 358.10, MTS Systems Corp., Eden Prarie, MN, USA).

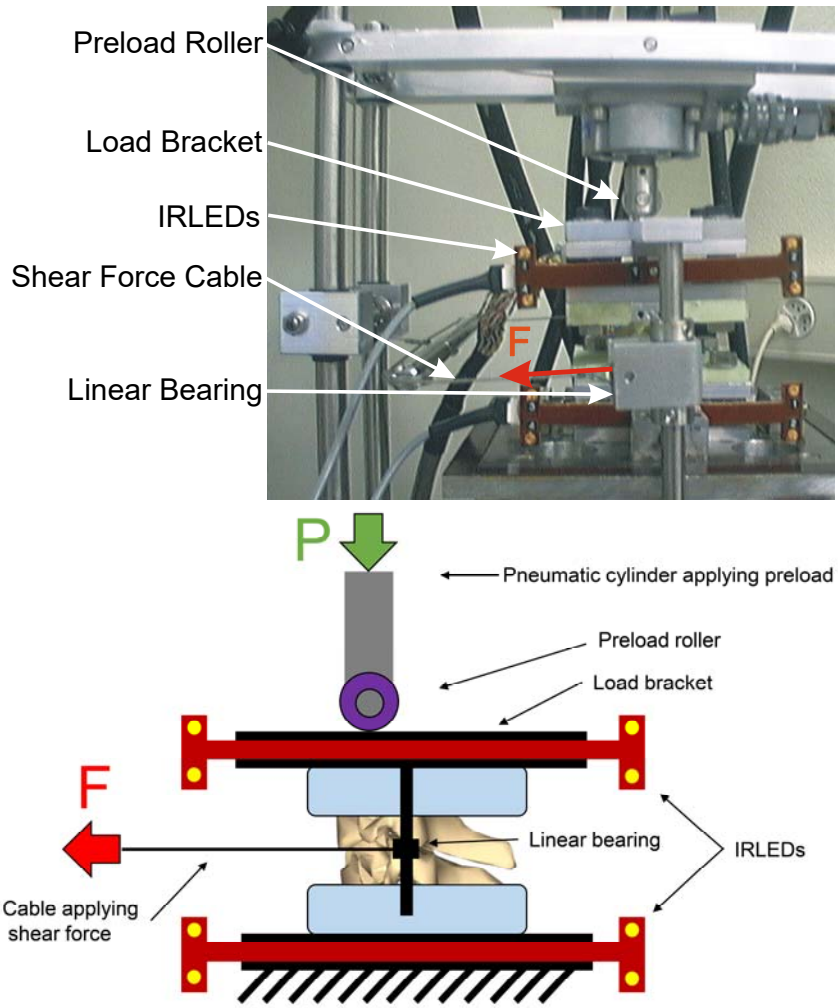

Fig. 1 Shear force application apparatus photographed (top) and schematic (bottom). The four markers (IRLEDs) mounted to the moulding material of each vertebra were used to capture motion. Anterior is left (same direction as force, F), and cranial is up. Steel cables were used to apply force to the cranial vertebra, F. The linear bearing was adjusted so that the shear force was applied in the mid-disc plane to achieve shear application. The pneumatic cylinder above the specimen was used to apply axial preload, P, through a roller which allowed specimen translation.

The caudal vertebra was rigidly fixed and the cranial vertebra was unconstrained. The testing machine actuator was attached to a steel cable to apply the shear force. The other end of the cable was attached to the load bracket fastened to the moulding material of the cranial vertebra. The point where the shear force was applied (F in Fig. 1) with respect to the FSU was continuously adjustable in the cranial-caudal direction using a linear bearing, which was

maintained at the mid-disc level. The applied shear force was measured using the testing machine load cell (Resolution < 1.0 N, model 661.19 F03, MTS Systems Corp., Eden Prairie, MN, USA). The load bracket and associated hardware was rotated about the specimen to achieve left, right, anterior and posterior shear loading without repositioning the specimen.

An initial shear force of approximately 20 N was applied and thereafter force was increased at 5 N/s to 200 N and held constant for 30 s, to allow viscoelastic effects to dissipate [27]. The force was then released at 5 N/s. Two preconditioning load cycles were applied and a third cycle was used for data collection [28]. Each direction of shear was first tested without axial preload and then with a constant preload of 200 N. The preload was applied using a pneumatic cylinder acting against the cranial vertebra loading fixture through a roller. The roller allowed anterior-posterior and lateral translation of the cranial vertebra (Fig. 1). Preload was initially applied such that a pure compressive displacement was achieved without any associated rotation. The magnitudes of shear and preload force were selected to represent *in vivo* physiologic, non-traumatic conditions up to loads experienced in low speed rear-end vehicle impacts [6,11].

Kinematics

An optoelectronic motion analysis system (Optotrak 3020, Northern Digital Inc., Waterloo, Canada) was used to track the relative motion of the cranial vertebra with respect to the caudal. Infrared light emitting diodes (IRLEDs) were attached to the cranial and caudal potting blocks (Fig. 1). The locations of the markers were recorded throughout the measurement cycle at a frequency of 10 Hz. The cranial and caudal vertebra coordinate systems were located at the centre of each endplate (inferior endplate of cranial vertebra, superior endplate of caudal vertebra) as determined from a lateral calibration x-ray. The location of the cranial vertebra's coordinate system with respect to the caudal vertebra's coordinate system was calculated in

terms of a three-dimensional translation vector and three ordered Euler angles using the ZYX ordering convention [29]. The positive z-axis refers to the anterior direction, the positive y-axis refers to the cranial direction and the positive x-axis refers to the left of the FSU.

Kinematics of the vertebral motion during shear force application was animated using previously published methods [30] to view the measured kinematics and for comparison to the computational model. Briefly, the vertebrae were CT scanned and segmented to generate three-dimensional geometric models. These geometric models were then registered to the initial positions of the vertebrae in the experimental tests using digitized optoelectric pointer data, transforming the original CT coordinate system to the optoelectric reference frame. The experimentally measured kinematics were then applied to the geometric models for animation.

Data analysis

Some experiments were removed from analysis due to faulty instrumentation as indicated in Table 1. In anterior shear with preload, pressure data from two specimens was removed. In posterior shear with preload, lateral mass strain data from one specimen was removed. In lateral shear with and without preload, data for one specimen was only available in right shear and not left shear. Further, in lateral shear without preload, lateral mass strain data from one specimen and pressure data from two specimens was removed. For lateral shear with preload, pressure data from two specimens was removed.

For anterior and posterior shear, the lateral mass strain gauge data were combined in the analysis. For lateral shear, left and right kinematic data, vertebral body strain data and pressure data were combined for analysis. Ipsilateral (same side as applied force) and contralateral (opposite side of applied force) lateral mass strain gauges were analysed separately in lateral shear.

Cubic smoothing spline interpolation with smoothing parameter of 0.9 was applied to the raw force-displacement data at 0.5 N increments using MATLAB. This allowed for direct comparison of pressure, strain and kinematic parameters at increasing shear force by removing multiple values of displacement for a single value of force which can occur in the raw experimental data. A mean experimental curve was then calculated at each 0.5 N increment. Shear stiffness was calculated for each specimen between 20 and 40 N and between 180 and 200 N of applied anterior and posterior shear. Under lateral shear, the shear stiffness was calculated between 100 and 120 N. These ranges of force represented regions within which the force-displacement relationships were typically linear. Linear regression analyses were applied to identify the best fit to the force-displacement data. An exemplar force-displacement curve showing the raw data, cubic smoothing spline interpolation and calculated stiffness ranges for specimen 1803 in anterior shear force application is pictured in Fig. S1 (online supplemental material).

Statistical power analyses indicated that an impracticably high number of specimens would be necessary to identify expected differences in strain quantities as statistically significant under the inter-specimen variance conditions. More than 16 specimens would have been necessary to detect differences in strain of 500 με with $p < 0.05$ under variance conditions typical of those measured (standard deviation = 500 με) [31]. Therefore, the strains were not analysed statistically.

Matched pair t-tests were used to identify differences in kinematic or pressure values while applying appropriate correction (Bonferroni) for multiple comparisons.

COMPUTATIONAL MODEL AND SIMULATION METHODS

Cervical spine model

Five motion segment models (C2-C3 through C6-C7) (Fig. 2) were extracted from a finite element neck model (GHBMC M50 version 5.0), approximating an average stature 50th percentile male. The cervical spine model geometry was generated from CT and MRI scans of 26-year-old male volunteer (stature: 174.9 cm, mass: 78.6 kg), scanned in an automotive seated position. The model geometry analysis, meshing, mesh quality analysis, and material characterization of the tissues were reported in Barker *et al.* [22]. The segment models were previously validated in extension and flexion for quasi-static and dynamic loading, and in axial bending and lateral bending for quasi-static loading and found to be in good agreement with the experimental data in extension, and slighter stiffer in flexion [22]. The models have not been assessed for pure shear loading.

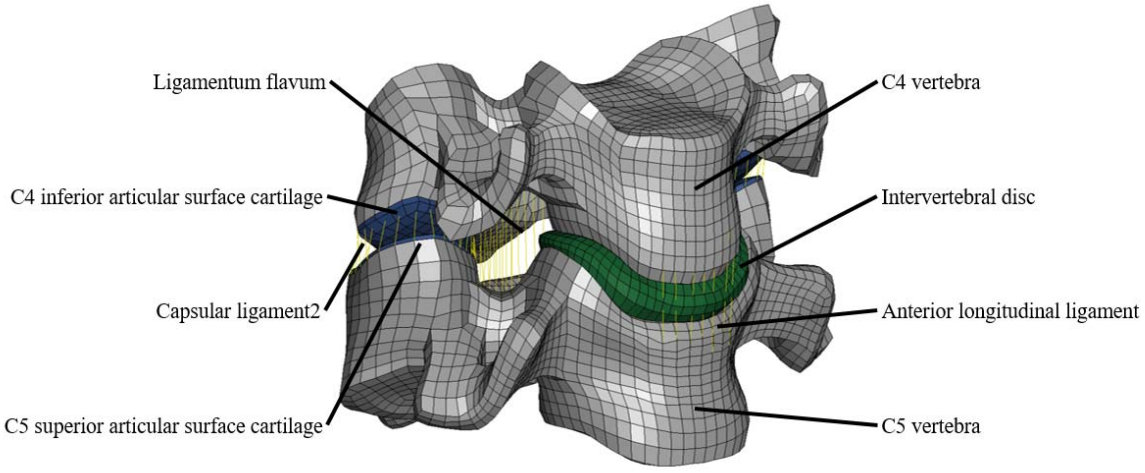

Fig. 2 C4-C5 motion segment finite element model.

Simulation procedures

The models were solved using an explicit finite element software (LS-DYNA MPP R9.2, LSTC, Livermore California), and results analysis was performed using a commercial post-processor (LS-PREPOST version 4.6).

The segment models were simulated in anterior shear, posterior shear, and lateral shear; with no preloading and with a 200 N compressive preload that was applied prior to shear loading. The axis system for the cranial and caudal vertebral bodies matched the axis system in the experimental procedure.

The inferior vertebra was fixed while the shear load and the compressive preload were applied to the unconstrained cranial vertebra. In the first set of simulations, shear loading from 0 N to 200 N was applied through the geometric centroid of the disc with no preload, as in the experiments. The shear load was applied along the Z axis (Fig. 3) for anterior and posterior shear, and it was applied in the X axis for lateral shear. In the second set, a compressive preload was applied from 0 N to 200 N as in the experiments, with the line of action passing through the geometric centroid of the disc. The compressive preload was held constant at 200 N while the shear load was applied from 0 N to 200 N in the same directions as the first set of simulations. The compressive preload was applied in the vertical Y axis.

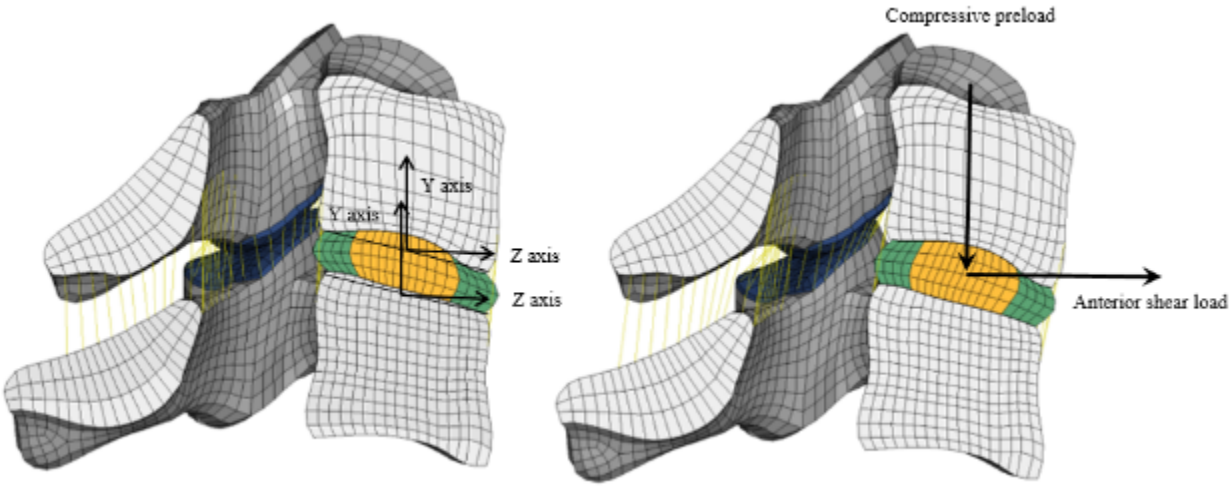

Fig. 3 Anterior shear without preload simulation at t = 0 (left) ms and t = 2000 ms (right) of the C4-C5 segment model. Axis system shown for C4 and C5 vertebrae (left): vertical axis (Y), anterior-posterior axis (Z), and lateral axis (X - into the page, not shown in image). The line of

action shown (right) for the shear load applied to the upper vertebra in the horizontal Z axis, and the compressive preload applied to the upper vertebra in the negative vertical Y axis

The kinematics in all three displacement and rotational axes were reported. The displacements were measured at the origin of the local coordinate system of the cranial vertebra (Fig. 3).

The maximum and minimum principal strains at the anterior face of the caudal vertebral body and on the lateral masses of the caudal vertebral were measured, at the locations of the strain gauges in the experimental testing. At the anterior face, the principal strains of twelve cortical bone shell elements were averaged, and on the lateral masses, the average of four cortical shell elements was reported.

The change in model disc pressure was measured by tracking the pressure in the nucleus pulposus. On initialization, the model assumed zero stress and pressure in all elements, including the nucleus. The model could accurately detect positive increases in pressure (compression), but has not been investigated for tensile pressure in the disc and therefore this was not reported.

Analysis

The computational model functional spinal unit responses were averaged and compared to the average responses obtained from the experimental data. Independent samples t-tests were used to compare the average model response to the experimental data applying Bonferroni correction for multiple comparisons.

RESULTS

Kinematics

Experimental data

In the experimental data, the largest motion responses were translations in the direction of the applied load (Table 2). Anterior shear was associated with flexion, which was reduced with the

addition of preload. Lateral shear without preload exhibited coupled rotation in all axes, while lateral shear with preload saw coupled rotations in lateral bending and axial torsion only. Anterior shear without preload caused the greatest shear translation. Preload caused a non-significant decrease in translation in anterior shear (31%) and non-significant increase in translation for lateral shear (27%). For posterior shear, preload significantly increased shear displacement (53%, p=0.001).

Animation frames at an applied shear load of 200 N for a typical specimen are shown in Fig. 4. Under anterior shear the facet joints were pressed into contact and the cranial vertebra was slightly flexed (Fig. 4). Under posterior shear the facet joints were distracted (Fig. 4). Under lateral shear an impingement of the cranial facet joint on the caudal lamina contralateral to the shear force application direction was identified (Fig. 4).

Table 2 Average (± standard deviation) main translations (underlined) and coupled rotations and translations for the experiments and computational model. T=translation, R=rotation, x is positive left, y is positive cranial, and z is positive anterior.

Applied Load		**T_x (mm)**	**T_y (mm)**	**T_z (mm)**	**R_x (°)**	**R_y (°)**	**R_z (°)**
Anterior	Experiment	0.03 (0.21)	0.63 (0.68)	<u>2.58 (0.95)</u>	3.35 (1.60)	-2.13 (2.80)	1.73 (3.54)
	Model	-0.00 (0.01)	0.11 (0.19)	<u>1.34 (0.35)</u>	2.51 (1.11)	0.01 (0.02)	0.01 (0.01)
Anterior + Preload	Experiment	0.21 (0.29)	0.34 (0.34)	<u>1.78 (0.86)</u>	0.94 (1.37)	-0.59 (1.28)	0.45 (0.50)
	Model	0.00 (0.01)	0.01 (0.03)	<u>0.95 (0.44)</u>	2.45 (1.43)	0.00 (0.02)	0.00 (0.02)
Posterior	Experiment	0.08 (0.22)	0.26 (0.28)	<u>-1.42 (0.51)</u>	2.56 (2.73)	-0.26 (0.70)	0.62 (0.89)
	Model	0.00 (0.00)	0.36 (0.24)	<u>-2.34 (0.25)</u>	1.91 (1.02)	-0.05 (0.04)	0.00 (0.01)
Posterior + Preload	Experiment	0.07 (0.14)	0.19 (0.25)	<u>-2.17 (0.74)</u>	1.00 (1.32)	-0.11 (0.99)	0.05 (0.24)
	Model	0.00 (0.01)	0.61 (0.19)	<u>-2.31 (0.39)</u>	4.49 (1.38)	-0.03 (0.07)	-0.03 (0.07)
Lateral	Experiment	<u>-1.12 (0.55)</u>	0.21 (0.42)	0.47 (0.41)	2.56 (2.23)	2.01 (1.24)	-1.92 (1.18)
	Model	<u>-2.28 (0.70)</u>	0.08 (0.09)	-0.07 (0.14)	0.59 (0.52)	1.13 (1.43)	-0.68 (0.84)
	Experiment	<u>-1.42 (0.63)</u>	0.20 (0.17)	0.10 (0.36)	-0.11 (0.26)	3.11 (1.87)	-3.34 (1.76)

Lateral + Preload	Model	-2.17 (0.87)	0.22 (0.05)	-0.10 (0.05)	1.21 (0.35)	1.21 (0.35)	-0.19 (1.04)

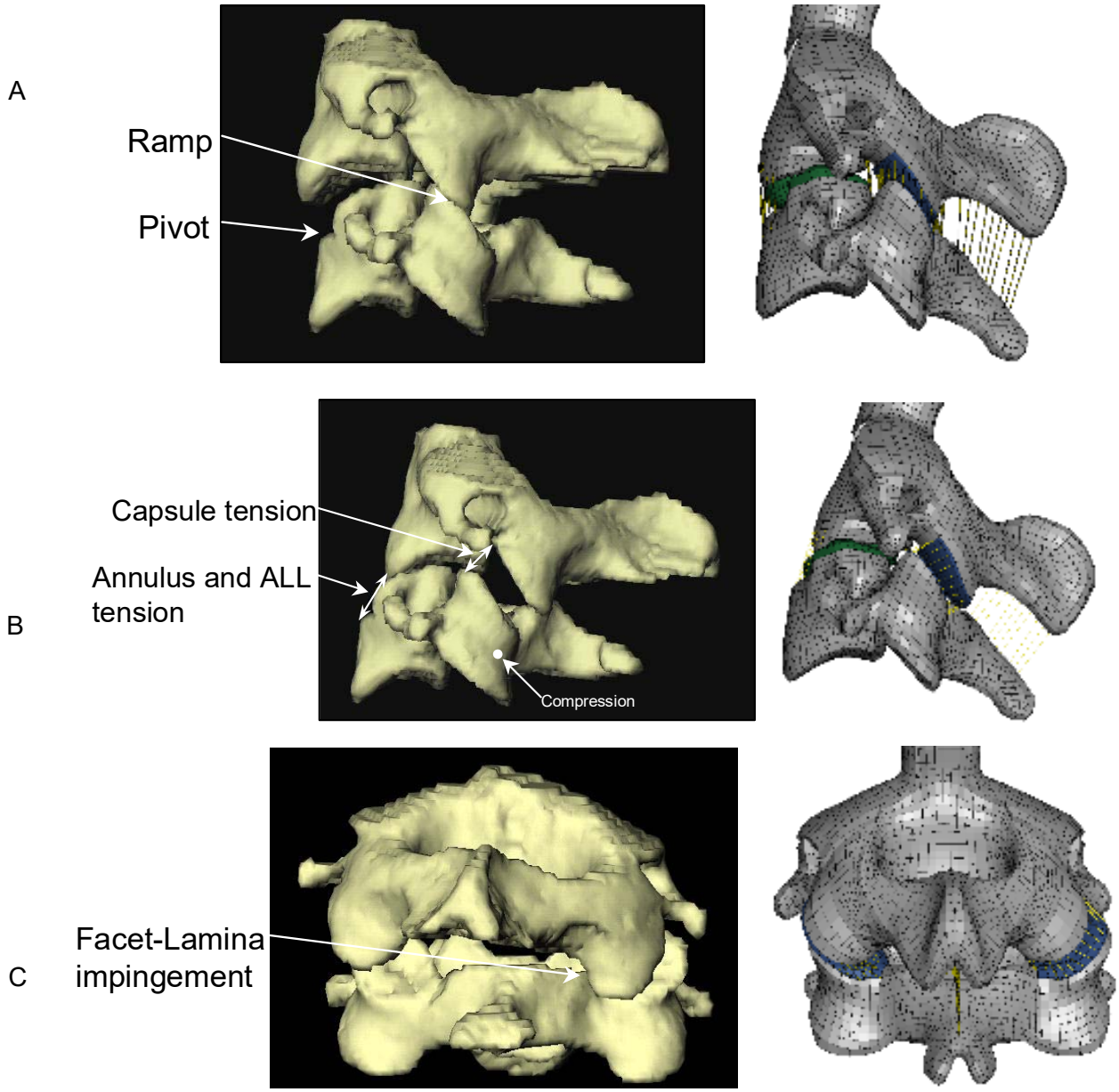

Fig. 4 Kinematics of a typical specimen (level C2-3) illustrated using reconstructed CT images (left) and corresponding FE model (right). The posture of the specimen under 200 N of shear force applied in the A) anterior, B) posterior and C) left-lateral directions. A) and B) are viewed from lateral and C) from posterior. The dens has been resected from C2 in the experiments to simplify moulding of the specimen. Hypothesized load-sharing mechanisms for each loading direction are illustrated on the reconstructed CT images.

Computational model

The predicted primary shear translations (as underlined in Table 2) were in good agreement between the model and experimental data. The model generally predicted lower average values for anterior shear, and higher average values for posterior and lateral shear compared to the experiments; however, there was no statistically significant difference between the model and experimental values ($p > 0.008$ corrected for multiple comparisons). The smaller anterior translation in anterior shear can be seen in Fig. 4 where the ramping of the superior facet joint is less pronounced at 200 N of shear force compared to the reconstructed experimental data. In lateral shear, the facet-lamina impingement hypothesized to influence the experimental response was not reproduced in the computational model (Fig. 4), potentially contributing to the larger average lateral translation.

Preload applied to the cervical spine model decreased shear translation in all shear directions. This decrease was consistent with the experimental findings in anterior shear, and contrary to the experimental response in posterior and lateral shear (see Table 2). In anterior and posterior shear, coupled rotations in the computational model occurred primarily in one axis (flexion-extension) with very little variance in other axis rotations compared to the experimental data. Flexion-extension rotations were significantly larger in the model compared to the experiments for the posterior shear with preload condition ($p = 0.001$). In lateral shear with preload, lateral bending rotation was significantly smaller ($p < 0.001$) and flexion-extension rotation was significantly larger ($p < 0.001$) in the model compared to the experimental data.

Shear Stiffness

Experimental data

The force-displacement relationships (e.g. Fig. A1, online supplemental material) were typically linear for the experimental data within the force ranges analysed (20-40 N and 180-200 N for anterior and posterior shear and 100-120 N for lateral shear). The average coefficients of determination (R^2) ranged from 0.92 (lateral shear no preload, 100-120 N) to 0.99 (posterior shear with preload, 180-200 N).

The increase in shear stiffness due to preload in anterior shear between 20-40 N was statistically significant ($p = 0.0036$), see Fig. 5. For posterior shear and anterior shear without preload, shear stiffness was higher at the larger shear forces (180-200 N) compared to the lower shear forces (20-40 N). This effect was only significant in anterior shear without preload ($p = 0.0007$). For shear forces between 20-40 N in the preload condition, stiffness was significantly smaller in posterior shear compared to anterior shear ($p = 0.0007$).

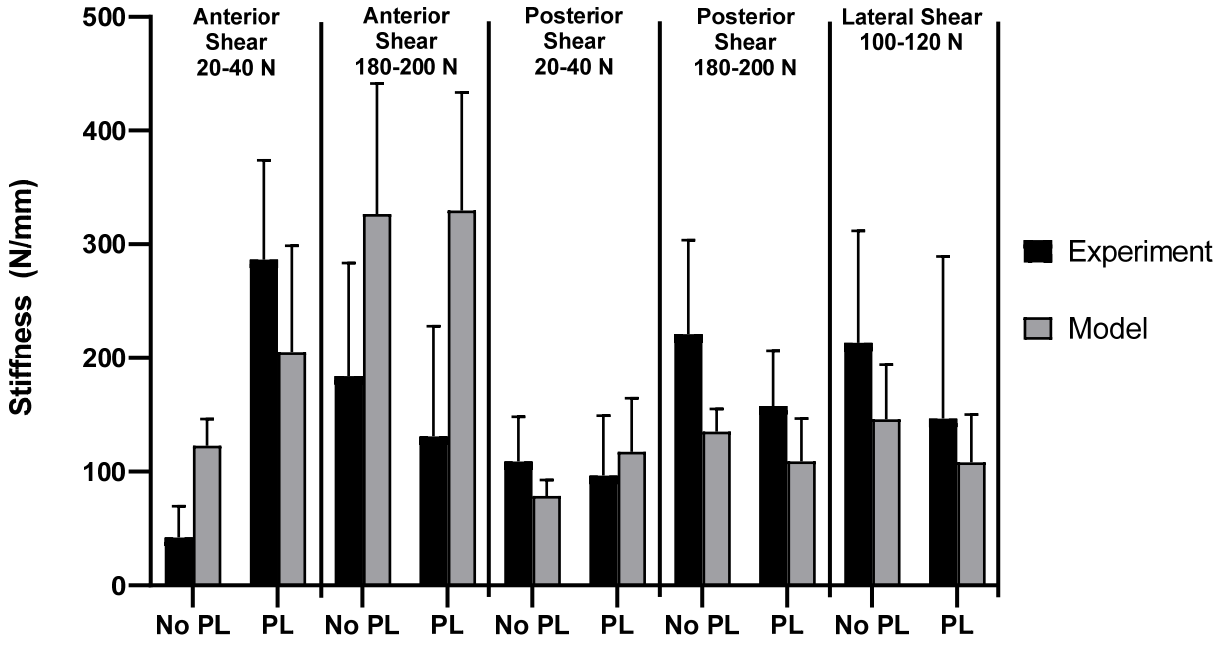

Fig. 5 Experimental and computational model shear stiffness values in anterior, posterior and lateral shear, calculated over the loading ranges specified for no preload (No PL) and preload (PL).

Computational model

The computational model force-displacement was also linear within the force ranges analysed, with average R^2 values ranging from 0.98 (posterior shear with preload 20-40 N), to 1.00 (anterior shear without preload 180-200 N, anterior shear with preload, posterior shear without preload, posterior shear with preload 180-200 N and lateral shear no preload 100-120 N). There were no statistically significant differences in the calculated stiffnesses compared to the experimentally measured stiffnesses, with the exception of anterior shear without preload, where a statistically significant difference was detected between the model and experimental data (20-40 N, p = 0004), see Fig. 5. The effect of preload was consistent with experimental data for anterior shear at 20-40 N, posterior shear 180-200 N and lateral shear 100-120 N. In anterior shear, preload caused an increased initial shear resistance (20-40 N) compared to the no preload condition, consistent with the experiments, but stiffness also increased at increasing force (180-200 N) contrary to the experimental results.

Bone Strain

Experimental data

For non-preloaded tests, the bone strains generally increased approximately linearly with increasing shear force application (see online supplemental material). Preload caused an initial bone strain, and the subsequent strain typically increased with increasing shear force.

In anterior shear, the greatest average strains were measured at the vertebral body (Fig. 6) and were compression dominated with the minimum (compressive, ε_2) principal strain 3.5 times that of the maximum (tensile, ε_1) principal strain. At the lateral masses, the maximum and minimum principal strains were approximately equal in magnitude, suggesting a shear-type strain

distribution. Preload decreased the average strain at the lateral masses and increased the compressive strain at the vertebral body.

Under posterior shear, the greatest average principal strains were measured at the lateral mass and were compression dominant ($\varepsilon_2=1.4\varepsilon_1$). At the vertebral body, tensile strain dominated ($\varepsilon_1=2.1\varepsilon_2$). Preload decreased strains at the lateral masses as well as shifted the strain field towards tensile dominated ($\varepsilon_1=1.8\varepsilon_2$) and caused dominant compressive strain fields at the vertebral body ($\varepsilon_2=3.2\varepsilon_1$).

Under lateral shear with no preload, the largest average strains were at the contralateral lateral mass. Lateral mass strain distributions were indicative of shear strain at all lateral shear and preload conditions. The vertebral body strain distribution was consistent with shear strain during lateral shear without preload. Preload caused a compression dominant strain field ($\varepsilon_2=1.9\varepsilon_1$).

Computational model

In general, strains generated at the vertebral body and lateral masses of the computational model FSUs show similar responses to the experimental data (Fig. 6). Strains increased approximately linearly with shear force application in non-preloaded tests and preload caused an initial strain that most often increased with shear force (see online supplemental material).

In contrast to the experimental data for anterior shear, the largest average strains were measured in the lateral masses (Fig. 6) and these were tensile strains ($\varepsilon_1=2.9\varepsilon_2$ both with and without preload). The vertebral strain was dominated by compression ($\varepsilon_2=2.3\varepsilon_1$ without preload, $\varepsilon_2=2.4\varepsilon_1$ with preload) consistent with experimental data but smaller in magnitude. Preload increased compressive strain at the vertebral body in anterior shear, consistent with experiments but the effect of preload differed at the lateral masses, where strain increased.

Under posterior shear without preload, the vertebral strains were tensile dominated ($\varepsilon_1=2.1\varepsilon_2$) and similar to the experimental data. These strains remained tensile dominated under preload ($\varepsilon_1=1.7\varepsilon_2$) while compression dominated strains were measured in the preload experiments. The lateral mass strains were smaller than experimental data in posterior shear.

Under lateral shear, the computational model exhibited small principal strains at the lateral masses compared to the experimental data. Vertebral body strains were more consistent with the experimental results, exhibiting a shear strain distribution under no preload and a compressive dominant strain field under preload ($\varepsilon_2=1.4\varepsilon_1$).

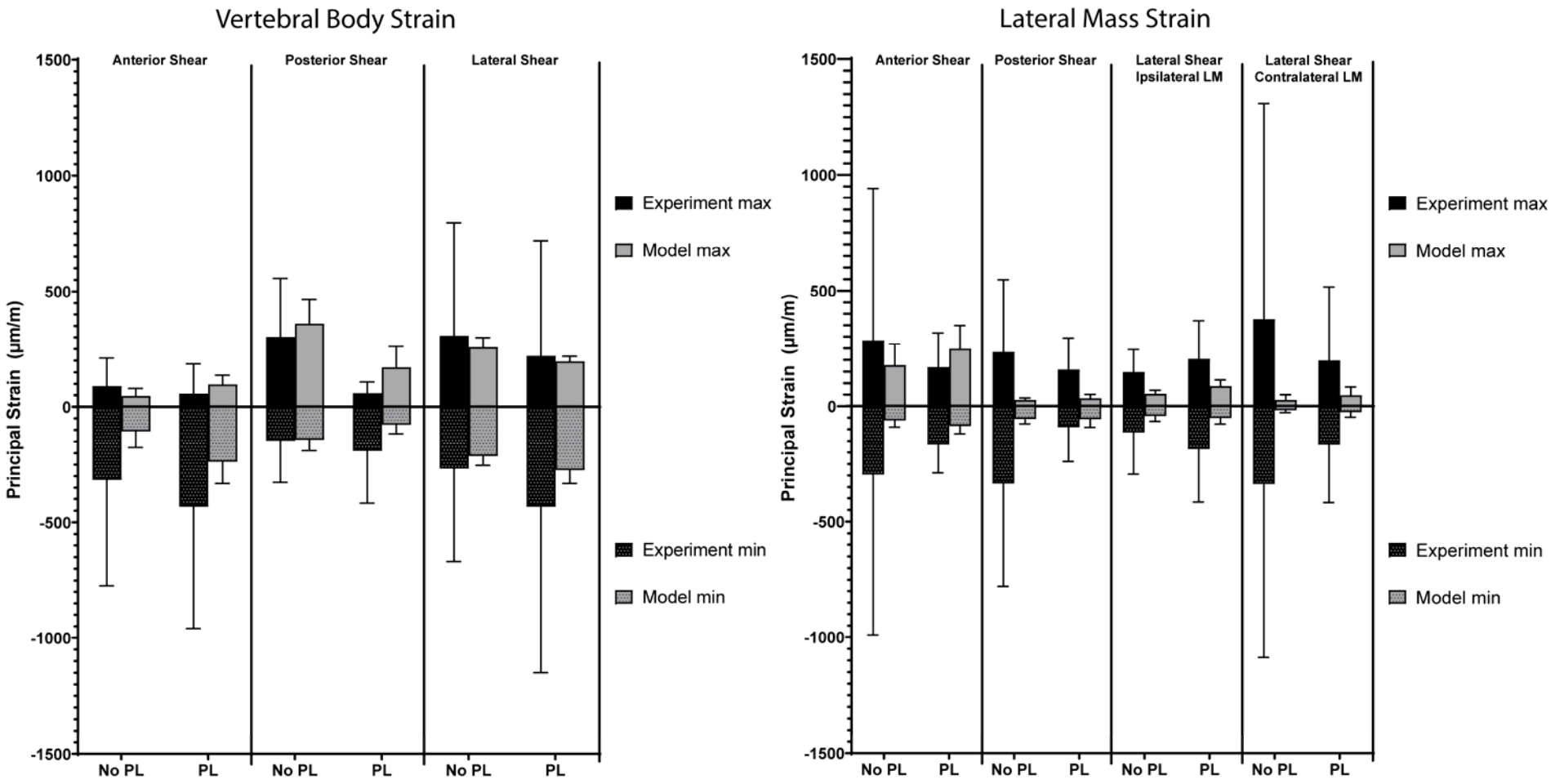

Fig. 6 Maximum and minimum principal strains at the vertebral body (left) and lateral masses (right) in the experiment and computational model in each shear direction.

Disc Pressure

Experimental data

Anterior shear without preload resulted in a small negative intradiscal pressure (Fig. 7), while posterior shear without preload resulted in a positive pressure. Preload positively increased pressure under all shear conditions. The largest pressure was recorded for posterior shear with preload (3.8 times greater than anterior shear with preload and 2.3 times greater than posterior shear without preload). Under lateral shear, positive disc pressures were measured and preload increased pressure by 3.6 times.

Disc pressure decreased upon application of anterior shear for both preload conditions, while contrastingly, disc pressure increased in each preload condition for both posterior and lateral shear (see online supplemental material).

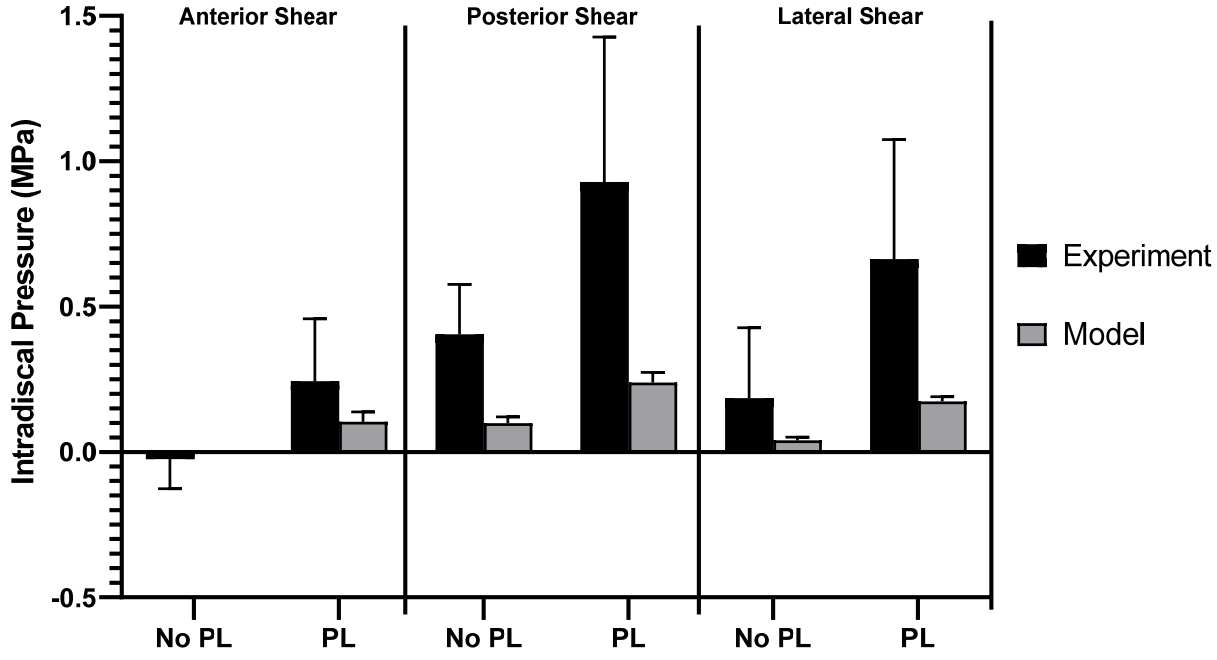

Fig. 7 Average intradiscal pressure at 200 N of applied shear.

Computational model

The measured disc pressure was negative under anterior shear without preload while the model predicted no disc pressure owing to the fluid model formulation used for the intervertebral disc. Disc pressure was positive for all other conditions (Fig. 7), consistent with the experimental results. The effect of preload was also consistent with the experimental data, causing a positive increase in pressure in all shear loading directions, see Fig. 7. The magnitude of intradiscal pressure was greater in the experiments compared to the model in all cases, but the trends in terms of changes in magnitude were similar for all cases. This difference was statistically significant in posterior shear with preload ($p = 0.003$) and lateral shear with preload ($p = 0.003$)

DISCUSSION

The first objective of this study was to experimentally characterise cervical spine kinematics and load-sharing mechanisms under shear force application, and the effect of preload. Our results suggest that an anterior shear force causes a "ramping" of the caudal facet joints on the cranial vertebra against the cranial facet joints on the caudal vertebra (Fig. 4A). This ramping was associated with a flexion rotation of the cranial vertebra, causing compression at the anterior vertebral body and shear strain at the lateral masses (Fig. 6). The cranial vertebra thus appeared to pivot about the compressed disc annulus anteriorly (Fig. 4A) and, in combination with the posterior ramping, resulted in a distraction of the intervertebral disc, anterior translation of the cranial vertebra (Table 2) and a decrease in disc pressure (Fig. 7 and Fig. S11 online supplemental material). The stiffness behaviour in anterior shear between 20-40 N was distinct from the other load levels and shear force directions. The stiffness without preload was much lower than that of the other load cases and preload increased stiffness by 6.8 times compared to a decrease in stiffness due to preload for the other load cases, suggesting preload engages a

mechanism for high initial resistance to anterior shear. Contact between the facet joints under the combined shear and compression is likely responsible for this behaviour as other directions of shear do not directly force the facets into contact. Preload also increased the compressive strain on the anterior vertebral body and reduced strain at the lateral masses indicating compression is preferentially transmitted through the anterior column. These findings support the role that anterior shear can play in cervical dislocation from head-first impacts, where spine compression is borne principally in the anterior column while shear force promotes local flexion and a first-order buckling response that can result in anterior dislocations in the lower cervical spine [2]. Posterior shear with preload resulted in predominantly posterior translation (Table 2), a decrease in compressive strain in the vertebral body (Fig. S19, online supplemental material), tensile strain at the lateral masses (Fig. 6) and a shear deformation to the intervertebral disc which resulted in an increase in disc pressure (Fig. 7 and Fig. S21, online supplemental material). Without preload, posterior shear caused tensile strain on the vertebral body (Fig. 6) likely transmitted through tension in the disc annulus and the anterior longitudinal ligament (Fig. 4B). A previous study found cutting the posterior ligaments of cervical spine segments did not change the shear stiffness in posterior shear however removal of the posterior bony elements entirely did reduce the posterior shear stiffness [12], suggesting a minimal role of tension in the facet capsule (Fig. 4B) in contributing to posterior shear stiffness. Notably, it is the distraction of the facet capsule, demonstrated to occur with posterior pure shear force application in this study (Fig. 4B), that leads to excessive strain in impact events and may be the cause of some WAD [32]. Lateral shear was transmitted as shear strain at the vertebral body and lateral masses (Fig. 6) resulting in increasing disc pressure (Fig. S27 and Fig. S33, online supplemental material) that reflects the absence of any disc distraction. The higher contralateral lateral mass shear strain

(Fig. 6) might suggest that force is being transmitted through the facet-lamina impingement and/or that the facet joint could "ramp" up the lamina in response (Fig. 4C), distracting the ipsilateral facet joint. This lateral shear response could be important in understanding the mechanism behind WAD being more severe and persistent in car occupants who had their head turned at the time of impact. A previous study showed greater capsular strains in cervical spine segments on the side of the neck that an occupant has their head turned towards [33]. Ipsilateral facet capsule distraction may be exacerbated in an oblique shear orientation consisting of combined posterior and lateral shear.

Of particular relevance to WAD is the observed stiffness decrease in posterior and lateral shear with preload potentially putting the spine at greater risk of injury. This effect was also observed in a previous study which applied posterior shear to cervical spines from C1 to T1 and suggested by the authors to occur due to loosening of ligaments [16]. However, this result was inconsistent with previous cervical segment tests that applied combined posterior shear, extension and axial compression, where there was a tendency toward decreased flexibility with increasing axial preload [11]. The difference may be the result of applying pure shear in this study rather than the combined loads chosen to reflect those present during rear-end collisions that might cause WAD.

A strength of this study is the application of pure shear forces to cervical functional spinal units as it is one of few studies to apply pure shear loading. Furthermore, the experimental conditions are ideal for replication in a computational environment allowing for validation of cervical spine finite element models as we were able to do here with the GHBMC model.

There are however a number of limitations associated with the experiments. Not all load transmission paths could be sensed with the instrumentation. This is a constraint imposed by the

difficulties inherent with applying sensors while preserving the anatomical structures and the segment biomechanics as much as possible.

The point of application of lateral shear force in the sagittal plane of the specimens was applied with a “force divider” which may have resulted in the resultant shear force being located in the center of the moulding block that was slightly posterior to the centre of the vertebral disc. Orientation of this force posterior to the disc centre may have contributed to the kinematic differences between the model and experimental data (Fig. 4C).

The bone strains exhibited large variation between specimens and therefore a statistical analysis was not possible. This may be partly due to variations in bone quality, vertebral anatomy and grouping of different spinal level specimens for analysis. The variation in our data was representative of that measured by other investigators [34,35].

The inter-subject variability inherent in testing biomechanical specimens also informed the decision to analyse the specimens together despite being from different levels of the spine. While the mechanical properties of the spine vary from level to level due to variations in geometry and structure, various segments are often grouped for analysis of biomechanical test data of this type [36–40] since inter-subject variability is typically greater than in grouping segment levels.

There are other limitations inherent to *ex vivo* testing, such as lack of muscle activation and inaccuracies in the biochemical and physical environment. Furthermore, it is not expected that pure shear loading occurs *in vivo*. However, applying isolated loads in the anatomical directions allows us to investigate important kinematic and load relationships caused by specific loads [5,6]. These data can also then be directly used to validate computational models.

Further limitations include the advanced age of the donor specimens and one donor with unknown information. While all specimens were scanned for and clear from disc abnormalities,

age related degenerative changes can occur to intervertebral discs and other tissues meaning the measured shear responses may not be representative of the general population.

Finite element cervical spine model shear response

The second objective of the study was to compare the experimental cervical spine shear response to the shear response of the GHBMC finite element neck model. This study is the first to assess the GHBMC model in shear loading, addressing the absence of experimental data appropriate and available for isolating the shear response of the cervical spine. Comparison of averaged computational functional spinal unit models generally showed good agreement with the kinematic, strains and disc pressures observed in the experiments. There were less coupled motions and smaller magnitudes of disc pressure and lateral mass strain in the finite element model compared to that seen experimentally, although the trends that occurred with preload application and different directions of shear force application were generally consistent.

The computational model provided some insights into the variability that could be anticipated based on load application. When preload was applied to the model, it could induce anterior or posterior motion, depending on three factors: the location along the A-P axis where the compressive preload was applied, the orientation of the segment (angle of the disc) relative to the global z axis, and the boundary condition/motion constraints on the vertebra. Such motions may explain variations in stiffness following the application of preload. An additional investigation where the preload was applied 5 mm anterior and posterior of the disc geometric centroid was conducted and resulted in approximately 0.2 mm difference in predicted shear displacement and 2 degrees in rotation. Although this effect was modest, these studies may explanation some of the variability in experimental results, with the limitation that the model was subject specific, and therefore did not address geometric variations that would be present in the experimental test data.

In the no preload condition, the computational model showed a smaller toe region in the force-displacement curve in anterior shear (Fig. S2, online supplemental material), and a larger toe region in posterior and lateral shear (Fig. S12 and Fig. S22, online supplemental material). In the experiments, application of a small initial force was necessary to reliably operate the materials testing machine which removed displacement that occurs around the neutral zone of the specimen. Therefore, the starting points at which the load is applied may slightly differ between the experiments and the computational model and explain some of the discrepancy in shear translation response.

The difference in shear stiffness in anterior shear, particularly at 180-200 N, may correspond to age related changes in the facets since facet contact contributes to resisting to anterior shear motion (Fig. 4A). The majority of experimental specimens were from donors confirmed over 80 years old whereas the computational model represents the anatomy of a 26-year-old 50th percentile male and incorporates material properties from younger samples (e.g. denser cortical bone) [22]. Facets undergo degenerative changes with aging, losing the ability to resist shear forces [41,42] and also experience a change in angle with increasing cervical spine lordosis associated with aging, and these factors are not reflected in the finite element model.

Quantifying strains in finite element models can be challenging due to sensitivity related to which elements are selected for analysis. In this study, elements were selected to closely approximate the location of the strain gauge sensor arrays in the experiments. Within the considerable variability of the strain results in the experimental data, the vertebral body strains measured in the computational model were in good agreement with the tested specimens. The strains measured at the lateral masses were smaller than those measured experimentally,

particularly in posterior and lateral shear and may be reflective of anatomical and structural differences between the computational model and the experimental specimens.

The intradiscal pressure was positive for all loading cases, except anterior shear where the pressure was approximately zero. The computational model predicted similar trends in disc pressure (Fig. 7), but with lower magnitude in all cases. The disc pressures are highly sensitive to compliance of the intervertebral disk such that a small change in compliance will have a large effect on pressure, and should be investigated further in the future.

In general, the computational model provided results in good agreement with the experimental data, considering that the models had not been previously assessed for pure shear loading. The general shape of the force vs. displacement curves matched the experimental data, especially in the primary shear direction. The vertebral body and lateral mass strain measurements matched well between the model and the experimental data. Model validation challenges included the effect of compressive preload on shear stiffness, and the contribution of the facet joint interaction on anterior shear stiffness, which could be related to the known variation of facet joint angle. Addressing these challenges will help our understanding of the model strengths and limitations, and improve the ability of the model to accurately predict injuries such as WAD due to low severity vehicle collisions, or facet joint dislocation due to high severity impacts.

CONCLUSION

This study identified the kinematics and major load-sharing mechanisms of the cervical spine under shear loading and characterised the influence of axial preload. The ramping of the facet joints and load sharing among the spinal column and posterior elements in anterior shear with and without preload provide new data for understanding to how anterior shear forces can contribute to facet dislocation injuries in the lower cervical spine. The basic biomechanics of the

cervical spine in posterior and lateral shear described by this study highlights the degree to which shear forces can distract the facet joints, a known occurrence in whiplash type injuries and potential contributor to acute and chronic pain resulting from rear-end collisions. Much of the observed experimental response was captured by a contemporary finite element model of the cervical spine, while areas to investigate further include the stiffness in anterior shear without preload and the magnitudes of disc pressure and load to the lateral masses.

CONFLICTS OF INTEREST / FUNDING

PAC works for a consulting company that may benefit from being associated with this work. None of the remaining parties have a conflict of interest with the submitted work.

REFERENCES

[1] Ivancic, P. C., 2012, "Head-First Impact with Head Protrusion Causes Noncontiguous Injuries of the Cadaveric Cervical Spine," Clin. J. Sport Med. Off. J. Can. Acad. Sport Med., **22**(5), pp. 390–396.

[2] Nightingale, R. W., Sganga, J., Cutcliffe, H., and Bass, C. R. 'Dale,' 2016, "Impact Responses of the Cervical Spine: A Computational Study of the Effects of Muscle Activity, Torso Constraint, and Pre-Flexion," J. Biomech., **49**(4), pp. 558–564.

[3] Siegmund, G. P., Myers, B. S., Davis, M. B., Bohnet, H. F., and Winkelstein, B. A., 2001, "Mechanical Evidence of Cervical Facet Capsule Injury during Whiplash: A Cadaveric Study Using Combined Shear, Compression, and Extension Loading," Spine, **26**(19), pp. 2095–101.

[4] Ivancic, P. C., Panjabi, M. M., and Ito, S., 2006, "Cervical Spine Loads and Intervertebral Motions during Whiplash," Traffic Inj Prev, **7**(4), pp. 389–99.

[5] Li, Y., Bishop, P. J., Wells, R. P., and McGill, S. M., 1991, "A Quasi-Static Analytical Sagittal Plane Model of the Cervical Spine in Extension and Compression," 35th STAPP car crash conference, San Diego, pp. 419–433.

[6] Moroney, S. P., Schultz, A. B., and Miller, J. A. A., 1988, "Analysis and Measurement of Neck Loads," J. Orthop. Res., **6**, pp. 713–720.

[7] Tencer, A. F., Mirza, S., and Bensel, K., 2002, "Internal Loads in the Cervical Spine during Motor Vehicle Rear-End Impacts: The Effect of Acceleration and Head-to-Head Restraint Proximity," Spine, **27**(1), pp. 34–42.

[8] Panjabi, M. M. ;, Summers, D. J. ;, Pelker, R. R. ;, Videman, T. ;, Friedlaender, G. E. ;, and Southwick, W. O., 1986, "Three-Dimensional Load-Displacement Curves Due to Forces on the Cervical Spine," J. Orthop. Res., **4**(2), pp. 152–61.

[9] Moroney, S. P., Schultz, A. B., Miller, J. A. A., and Andersson, G. B. J., 1988, "Load-Displacement Properties of Lower Cervical Spine Motion Segments," J. Biomech., **21**(9), pp. 769–779.

[10] Shea, M., Edwards, W. T., White, A. A., and Hayes, W. C., 1991, "Variations of Stiffness and Strength along the Human Cervical Spine," J. Biomech., **24**(2), pp. 95–107.

[11] Siegmund, G. P., Myers, B. S., Davis, M. B., Bohnet, H. F., and Winkelstein, B. A., 2000, "Human Cervical Motion Segment Flexibility and Facet Capsular Ligament Strain under Combined Posterior Shear, Extension and Axial Compression," Stapp Car Crash J., **44**, pp. 159–170.

[12] Dowling-Medley, J. J., Doodkorte, R. J., Melnyk, A. D., Cripton, P. A., and Oxland, T. R., 2020, "Shear Stiffness in the Lower Cervical Spine: Effect of Sequential Posterior Element Injury," Proc. Inst. Mech. Eng. [H], **234**(2), pp. 141–147.

[13] Cripton, P. A., Berlemann, U., Visarius, H., Begeman, P., and Prasad, P., 1995, "Response of the Lumbar Spine Due to Shear Loading," Soc. Automot. Eng. SP-1077, **Paper#950662**.

[14] Liu, Y. K., Ray, G., and Hirsch, C., 1975, "The Resistance of the Lumbar Spine to Direct Shear," Orthop. Clin. North Am., **6**(1), pp. 33–48.

[15] Panjabi, M. M., White, A. A., and Johnson, R. M., 1975, "Cervical-Spine Mechanics as a Function of Transection of Components," J. Biomech., **8**(5), pp. 327–336.

[16] Yang, K., Begeman, P., Muser, M., Niederer, P., and Walz, F., 1997, "On the Role of Cervical Facet Joints in Rear End Impact Neck Injury Mechanisms," *SAE International Congress and Exposition*, SAE, Detroit, Michigan.

[17] Cronin, D., Singh, D., Gierczycka, D., Barker, J., and Shen, D., 2018, "Chapter 13: Modeling the Neck for Impact Scenarios," *Basic Finite Element Method and Analysis as Applied to Injury Biomechanics*, K. Yang, ed., Elsevier Inc., London, UK, pp. 503–538.
[18] Goel, V. K., and Clausen, J. D., 1998, "Prediction of Load Sharing among Spinal Components of a C5-C6 Motion Segment Using the Finite Element Approach," Spine, **23**(6), pp. 684–691.
[19] Kumaresan, S., Yoganandan, N., and Pintar, F. A., 1999, "Finite Element Analysis of the Cervical Spine: A Material Property Sensitivity Study," Clin. Biomech., **14**(1 JAN), pp. 41–53.
[20] Panzer, M. B., and Cronin, D. S., 2009, "C4–C5 Segment Finite Element Model Development, Validation, and Load-Sharing Investigation," J. Biomech., **42**(4), pp. 480–490.
[21] Mustafy, T., El-Rich, M., Mesfar, W., and Moglo, K., 2014, "Investigation of Impact Loading Rate Effects on the Ligamentous Cervical Spinal Load-Partitioning Using Finite Element Model of Functional Spinal Unit C2–C3," J. Biomech., **47**(12), pp. 2891–2903.
[22] Barker, J. B., Cronin, D. S., and Nightingale, R. W., 2017, "Lower Cervical Spine Motion Segment Computational Model Validation: Kinematic and Kinetic Response for Quasi-Static and Dynamic Loading," J. Biomech. Eng., **139**(6).
[23] Ng, H. W., Teo, E. C., and Lee, V. S., 2004, "Statistical Factorial Analysis on the Material Property Sensitivity of the Mechanical Responses of the C4–C6 under Compression, Anterior and Posterior Shear," J. Biomech., **37**(5), pp. 771–777.
[24] Barker, J., and Cronin, D., 2020, "Multi-Level Validation of a Male Neck Finite Element Model with Active Musculature," J. Biomech. Eng., **Accepted May 10, 2020**.
[25] Cronin, D. S., 2014, "Finite Element Modeling of Potential Cervical Spine Pain Sources in Neutral Position Low Speed Rear Impact," J. Mech. Behav. Biomed. Mater., **33**, pp. 55–66.
[26] Cripton, P. A., Dumas, G. A., and Nolte, L., 2001, "A Minimally Disruptive Technique for Measuring Intervertebral Disc Pressure in Vitro: Application to the Cervical Spine," J.Biomech., **34**(4), pp. 545–549.
[27] Pelker, R. R., Duranceau, J. S., and Panjabi, M. M., 1991, "Cervical Spine Stabilization. A Three-Dimensional, Biomechanical Evaluation of Rotational Stability, Strength, and Failure Mechanisms," Spine, **16**(2), pp. 117–122.
[28] Panjabi, M. M., 1988, "Biomechanical Evaluation of Spinal Fixation Devices: I. A Conceptual Framework," Spine, **13**(10), pp. 1129–1134.
[29] Small, C. F., Bryant, J. T., and Pichora, D. R., 1992, "Rationalization of Kinematic Descriptors for Three-Dimensional Hand and Finger Motion," J. Biomed. Eng., **14**, pp. 133–141.
[30] Cripton, P. A., Sati, M., Orr, T. E., Bourquin, Y., Dumas, G. A., and Nolte, L. P., 2001, "Animation of in Vitro Biomechanical Tests," J. Biomech., **34**(8), pp. 1091–1096.
[31] Lieber, R. L., 1994, "Experimental Design and Statistical Analysis," *Orthopaedic Basic Science*, American academy of orthopaedic surgeons, Rosemont, IL.
[32] Siegmund, G. P., Winkelstein, B. A., Ivancic, P. C., Svensson, M. Y., and Vasavada, A., 2009, "The Anatomy and Biomechanics of Acute and Chronic Whiplash Injury," Traffic Inj. Prev., **10**(2), pp. 101–112.
[33] Siegmund, G. P., Davis, M. B., Quinn, K. P., Hines, E., Myers, B. S., Ejima, S., Ono, K., Kamiji, K., Yasuki, T., and Winkelstein, B. A., 2008, "Head-Turned Postures Increase the Risk of Cervical Facet Capsule Injury During Whiplash:," Spine, **33**(15), pp. 1643–1649.

[34] Buttermann, G. R., Kahmann, R. D., Lewis, J. L., and Bradford, D. S., 1991, "An Experimental Method for Measuring Force on the Spinal Facet Joint: Description and Application of the Method," J.Biomech.Eng., **113**(4), pp. 375–386.
[35] Pintar, F. A., Yoganandan, N., Pesigan, M., Reinartz, J., Sances, A. Jr., and Cusick, J. F., 1995, "Cervical Vertebral Strain Measurements under Axial and Eccentric Loading," J. Biomech. Eng., **117**, pp. 474–478.
[36] Whyte, T., Melnyk, A. D., Van Toen, C., Yamamoto, S., Street, J., Oxland, T. R., and Cripton, P. A., 2020, "A Neck Compression Injury Criterion Incorporating Lateral Eccentricity," Sci. Rep., **10**(1), p. 7114.
[37] Panjabi, M. M., Oxland, T. R., and Parks, E. H., 1991, "Quantitative Anatomy of the Cervical Spine Ligaments. Part II. Middle and Lower Cervical Spine," J. Spinal Disord., **4**(3), pp. 277–285.
[38] Panjabi, M. M., Duranceau, J., Goel, V. K., Oxland, T. R., and Takata, K., 1991, "Cervical Human Vertebrae: Quantitative Three-Dimensional Anatomy of the Middle and Lower Regions," Spine, **16**(6), pp. 861–869.
[39] Van Toen, C., Melnyk, A. D., Street, J., Oxland, T. R., and Cripton, P. A., 2014, "The Effect of Lateral Eccentricity on Failure Loads, Kinematics, and Canal Occlusions of the Cervical Spine in Axial Loading," J. Biomech., **47**(5), pp. 1164–1172.
[40] Melnyk, A., Whyte, T., Thomson, V., Marion, T., Yamamoto, S., Street, J., Oxland, T. R., and Cripton, P. A., 2020, "The Effect of Compression Applied Through Constrained Lateral Eccentricity on the Failure Mechanics and Flexibility of the Human Cervical Spine," J. Biomech. Eng., **142**(101005).
[41] Kettler, A., Werner, K., and Wilke, H.-J., 2007, "Morphological Changes of Cervical Facet Joints in Elderly Individuals," Eur. Spine J., **16**(7), pp. 987–992.
[42] Papadakis, M., Sapkas, G., Papadopoulos, E. C., and Katonis, P., 2011, "Pathophysiology and Biomechanics of the Aging Spine," Open Orthop. J., **5**, pp. 335–342.

FIGURE CAPTION LIST

Fig. 1 Shear force application apparatus photographed (top) and scehmatic (bottom). The four markers (IRLEDs) mounted to the moulding material of each vertebra were used to capture motion. Anterior is left (same direction as force, F), and cranial is up. Steel cables were used to apply force to the cranial vertebra, F. The linear bearing was adjusted so that the shear force was applied in the mid-disc plane to achieve pure shear application. The pneumatic cylinder above the specimen was used to apply axial preload, P, through a roller which allowed specimen translation.

Fig. 2 C4-C5 motion segment finite element model.

Fig. 3 Anterior shear without preload simulation at t = 0 (left) ms and t = 2000 ms (right) of the C4-C5 segment model. Axis system shown for C4 and C5 vertebrae (left): vertical axis (Y), anterior-posterior axis (Z), and lateral axis (X - into the page, not shown in image). The line of action shown (right) for the shear load applied to the upper vertebra in the horizontal Z axis, and the compressive preload applied to the upper vertebra in the negative vertical Y axis

Fig. 4 Kinematics of a typical specimen (level C2-3) illustrated using reconstructed CT images (left) and corresponding FE model (right). The posture of the specimen under 200 N of shear force applied in the A) anterior, B) posterior and C) left-lateral directions. A) and B) are viewed from lateral and C) from posterior. The dens has been resected from C2 in the experiments to simplify moulding of the specimen. Hypothesized load-sharing mechanisms for each loading direction are illustrated on the reconstructed CT images.

Fig. 5 Experimental and computational model shear stiffness values in anterior, posterior and lateral shear, calculated over the loading ranges specified for no preload (No PL) and preload (PL).

Fig. 6 Maximum and minimum principal strains at the vertebral body (left) and lateral masses (right) in the experiment and computational model in each shear direction.

Fig. 7 Average intradiscal pressure at 200 N of applied shear.

TABLE CAPTION LIST

Table 1 Specimen details and experimental data collected for each specimen (VB is vertebral body, LM is lateral mass, Pre is axial preload, A is anterior shear, P is posterior shear, L is left shear, R is right shear)

Table 2 Average (± standard deviation) main translations (underlined) and coupled rotations and translations for the experiments and computational model. T=translation, R=rotation, x is positive left, y is positive cranial, and z is positive anterior.